Nearly Perfect Spin Filter Based on a Wire of Half-Metallic $(\eta^5\text{-}C_5H_5)Ti(\eta^8\text{-}C_8H_8)Ti$ Units

Sicong Zhu,[1,2] Jianming Fang,[1] Kailun Yao,[1] and Yanqing Wu[1,2,*]

[1]*Wuhan National High Magnetic Field Center and School of Physics, Huazhong University of Science and Technology, Wuhan 430074, China*

[2]*School of Electrical and Electronic Engineering, Huazhong University of Science and Technology, Wuhan 430074, China*

(Received 9 March 2015; revised manuscript received 21 May 2015; published 27 July 2015)

Organic molecular devices show strong potential for future nanoelectronics applications, many of which require multifunction capability. Organometallic $[(C_5H_5)Ti(C_8H_8)]_n$ clusters are one of the few molecular material clusters that have been synthesized experimentally. Here we present a theoretical study of the spin-polarized transport on the clusters of $[(C_5H_5)Ti(C_8H_8)]_n$ by using nonequilibrium Green's functions combined with the density-functional theory. Results indicate that one-dimensional, organic $(\eta^5\text{-}C_5H_5)Ti(\eta^8\text{-}C_8H_8)Ti$ wire has unique half-metallic properties with 100% spin polarization near the Fermi level in the ground state. We predict that finite-layer $[(C_5H_5)Ti(C_8H_8)]_n$ clusters coupled to gold electrodes exhibit a near-perfect spin-filter effect. Furthermore, due to the large spin coherence originated from its organic nature, these devices possess a spin-valve effect with large magnetoresistance. Our findings suggest that such a multifunctional molecular device is an excellent candidate for future molecule-based spintronic applications.

DOI: 10.1103/PhysRevApplied.4.014019

I. INTRODUCTION

Organic molecules have attracted much attention in recent years due to their potential applications in nanoelectronics and spintronics, including spin filters, molecular rectification, field-effect characteristics, and negative differential resistance [1–11]. In particular, the spin-filter phenomenon allows one to obtain highly spin-polarized charge carriers generated from nonmagnetic electrodes using magnetic tunnel barriers. A large tunneling magnetoresistance can be realized in a wide bias range due to the effective control of spin-polarized transport under an external magnetic field [12]. This tunneling magnetoresistance in organic molecular devices has great potential in applications such as magnetic recording, memory, and other fields involving spin electronics.

The organometallic-iron (Fe) compound was first synthesized *via* chemical reactions in 1950, which is composed of a Fe atom sandwiched between two parallel cyclopentadienyl (Cp) rings ($FeCp_2$), named ferrocene. Soon afterwards, numerous ferrocenelike organometallic compounds were successfully synthesized, in which the vanadium-benzene (VBz) multidecker molecular wires have half-metallic and perfect spin-filtering effects [13–17]. Experimentally, the multidecker structures of the vanadium, Fe, and Cp are produced by the laser valorization of V and $FeCp_2$ targets. Recent studies show that the finite one-dimensional FeCp multidecker molecule sandwiched between two ferromagnetic electrodes shows a half-metallicity and the perfect spin-filtering property. Its current-voltage curves exhibit negative differential resistance [18]. Yang *et al.* investigate a bias-controlled giant magnetoresistance (GMR) effect in a finite one-dimensional FeCp multidecker molecule sandwiched between two ferromagnetic cobalt electrodes. The highest GMR can reach $(2.0 \times 10^4)\%$ [19]. Wang *et al.* show that the one-dimensional infinite VCp, VBzVCp (Bz = benzene), and V_2 Ant (Ant = anthracene) have ferromagnetic half-metallic properties, and a perfect spin-filtering effect could also be further achieved when the finite VCp and $VFeCp_2$ are coupled to gold electrodes [20]. In addition, the infinite one-dimensional vanadium-cyclooctatetraene (V-COT) wire also has half-metallic properties. When the finite one-dimensional V-COT wire is coupled to gold electrodes, a nearly perfect spin-filtering effect is achieved [21]. However, the experimental stability of the organic metal that constructed multifunctional devices needs to be further explored.

Very recently, the vital importance of π-carbocylic ligands such as $\eta^5\text{-}C_5H_5$ and $\eta^6\text{-}C_6H_6$ (hapticity η^n describes a ligand that coordinates through n contiguous atoms) in organometallic chemistry and their bonding to transition metals is well acknowledged [22–30]. The chemistry of mixed sandwich complexes $C_5H_5MC_8H_8$ containing both five- and eight-membered rings was first studied by Nakamura and Hagihara [31]. Discovered later by Van Oven and de Liefde Meijer [32] in 1969, the titanium derivative $(\eta^5\text{-}C_5H_5)Ti(\eta^8\text{-}C_8H_8)$ is the first synthesized sandwich compound containing parallel five- and eight-membered rings, as a product from the reaction of

*yqwu@mail.hust.edu.cn

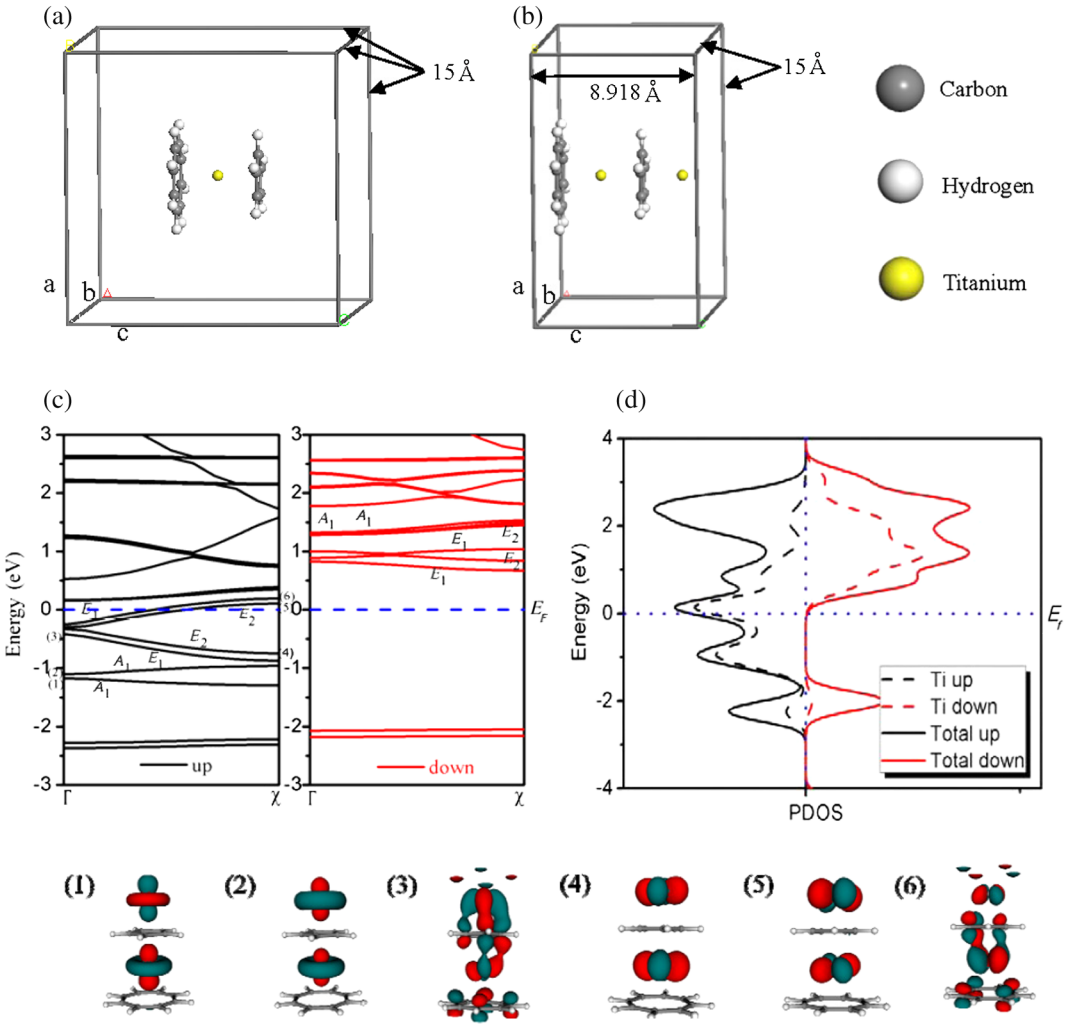

FIG. 1. Structure optimization models. (a) The sandwich compounds $C_5H_5TiC_8H_8$. (b) The infinite SMW model with eclipsed configurations. Yellow spheres denote titanium atoms, dark gray spheres denote carbon atoms, and small light gray spheres denote hydrogen atoms. (c) Computed band structure of the infinite $[C_5H_5TiC_8H_8Ti]_\infty$. Left flat: spin up. Right flat: spin down. The labels (1)–(6) under the band structure refer to crystalline orbitals of the wire calculated for the Γ point. (c) The computed partial density of states (PDOS) of the infinite $[C_5H_5TiC_8H_8Ti]_\infty$.

$K_2C_8H_8$ with $(\eta^5\text{-}C_5H_5)TiCl_3$ or $(\eta^5\text{-}C_5H_5)_2TiCl_2$ [32]. The parallel sandwich structure of this product, shown in Fig. 1(a), was confirmed later with x-ray diffraction by other researchers [7]. Moreover, as investigated by the density-functional theory (DFT) calculation [33], the octahapto parallel ring sandwich $(\eta^5\text{-}C_5H_5)Ti(\eta^8\text{-}C_8H_8)$ exhibits the lowest energy structure among the complexes $C_5H_5MC_8H_8$ (M = Ti, V, Cr, Mn, Fe, Co, or Ni). Recently, research on the π-hydrocarbon ligand $(\eta^5\text{-}C_5H_5)Ti(\eta^8\text{-}C_8H_8)$ chemistry has advanced with the ability to vary the bridging moiety, allowing a wide variety of these species to be realized [34].

II. METHOD AND STRUCTURE

In this study, we perform calculations on the electronic and magnetic properties of one-dimensional organometal $(\eta^5\text{-}C_5H_5)Ti(\eta^8\text{-}C_8H_8)Ti$ with infinite length. As shown in Fig. 1(b), the crystal lattice constant is 8.918 Å after optimization. In this work, we focus on the spin transport of the multilayer clusters $[(C_5H_5)\,Ti\,(C_8H_8)]_n$ sandwiched between two Au(100) surfaces.

Calculations on crystal properties are performed by using the DEMOL^3 code of Materials Studio developed by Accelrys [35]. We use quantum transport package ATK [36–38], in which DFT is carried out within the Keldysh nonequilibrium Green's function (NEGF) formalism [39,40]. The exchange correlation function is treated within the generalized gradient approximation (GGA) with the Perdew-Burke-Ernzerhof functional. The Monkhorst-Pack scheme k-point grid sampling is set at $1 \times 1 \times 100$ for the Brillouin zone. Convergence parameters are selected as follows: total energy tolerance 1×10^{-5} eV/atom and

maximum force tolerance 0.05 eV/nm. We assume $T = 300$ K on the left and right electrodes on the device when we calculate the spin transport of the system. Geometrical optimization is also performed. Atomic cores are defined by standard, nonlocal, norm-conserving pseudopotential methods. The exchange correlation is treated at the GGA level. We use an s, p, d LCAO basis set in our calculations. The self-consistent NEGF DFT is controlled by a numerical tolerance of 10^{-4} eV. The spin-polarized current is calculated by using

$$I_\sigma = \frac{e}{h}\int_{+\infty}^{-\infty} T_\sigma(E, V_b)[f_l(E-\mu_L) - f_r(E-\mu_R)]dE, \tag{1}$$

where f is the Fermi-Dirac distribution and $T_\sigma(E, V_b)$ is the transmission coefficient for the spin channel at the energy E and the bias voltage V_b. $f_{l/r}(E, V_b)$ is the equilibrium Fermi distribution for the left or right electrode. Effectively, the difference of $f_l(E, V_b)$ and $f_r(E, V_b)$ is well defined in an energy window corresponding to the applied bias around the average Fermi level.

Not only GGA but also local density approximation (LDA) has always been used to predict the properties of one-dimensional organic $(\eta^5\text{-}C_5H_5)Ti(\eta^8\text{-}C_8H_8)Ti$ wire and clusters. We also calculate the electronic structures and transport properties of the $[(C_5H_5)Ti(C_8H_8)]_n$ by LDA. The results show that the band structure of the $(\eta^5\text{-}C_5H_5)Ti(\eta^8\text{-}C_8H_8)Ti$ wire calculated by LDA are very similar to those obtained by GGA, which results in the same half-metallic property. So we show only the results corresponding to GGA.

III. RESULTS AND DISCUSSION

The band structure shown in Fig. 1(c) reveals that the sandwich molecular wire (SMW) is half-metallic and that the spin-majority channel is metallic, while the spin-minority channel is semiconducting. We supplement the corresponding energy level (1)–(6) near the Fermi surface by plotting the crystalline orbitals at the Γ point. As shown in Fig. 1(d), the partial DOS indicates the half-metallic behavior is mainly contributed by the Ti 3d orbital. Further examination of magnetic properties shows that the magnetic moment of $[(\eta^5\text{-}C_5H_5)Ti(\eta^8\text{-}C_8H_8)Ti]_\infty$ is strikingly different from that expected from the valence electron configuration of the Ti atom. Further investigation shows that, under the strong crystal field in this structure, the 3d orbitals of the two Ti split into two $d_{3z^2\text{-}r^2}(A_1)$ [marked as 1 and 2 in Fig. 1(b)] orbitals and four sets of degenerated orbitals d_{xy}, $d_{x^2\text{-}y^2}$ (E_2) [marked as 4 and 5 in Fig. 1(b)] and d_{xz}, d_{yz} (E_1) [marked as 3 and 6 in Fig. 1(b)].

In the $3d^24s^2$ electronic configuration of the Ti-based valence electron atom, Cp (Cp, C_5H_5) and COT (COT, C_8H_8) are metastable radicals, and the two five-membered and eight-membered rings possess five and eight p electrons, respectively. According to the Huckel rule, the rings tend to capture extra electrons to form a stable, aromatic system with $4m + 2$ electrons (where m is an integer). As a result, the Cp captures one electron from the Ti atom to the ligand upon C_5H_5 coordination, while the COT captures two of them from the Ti atom to C_8H_8, which leads to the system being configured as $[COT^{2-}Ti^{2+}Cp^{1-}Ti^{1+}]_\infty$.

The remaining five valence electrons of the two Ti occupy the d degenerated orbitals in $[(C_5H_5)Ti(C_8H_8)Ti]$. Because of strong hybridization, the split energy level of the spin-down 3d orbitals is greater than that of the spin-up ones [Fig. 1(c)]. The five majority (spin-up) electrons occupy the A_1, E_1, and E_2 orbitals first, leaving five unpaired electrons in the orbitals. In such a case, the magnetic moment of $[(C_5H_5)Ti(C_8H_8)Ti]$ should be 5.0 μB per unit cell, which is consistent with our first-principles calculation.

The unusual electronic properties of the infinite 1D wire remain unchanged in molecules with finite length. As an example, we now show how these molecular wires act as

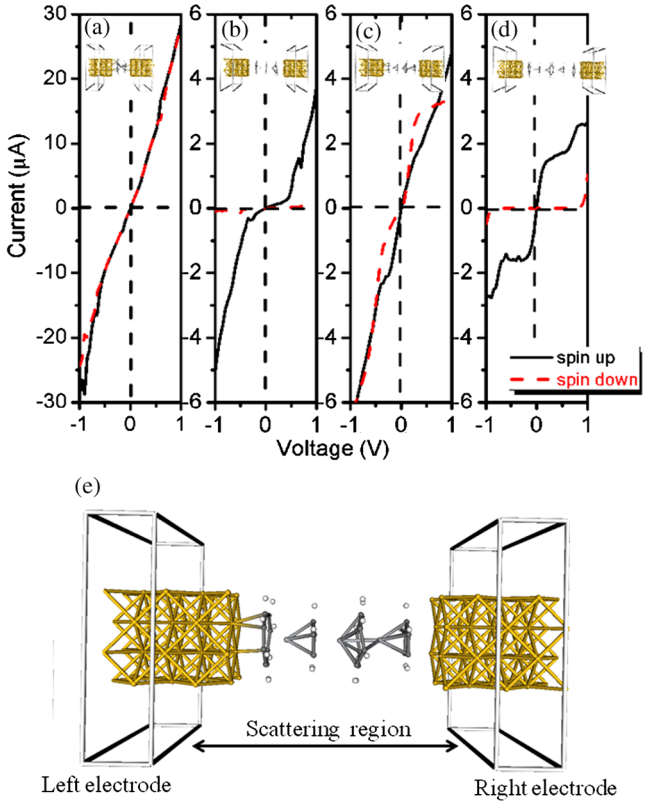

FIG. 2. Spin-polarized I-V curves for (a) cluster $Ti_1:(C_8H_8)Ti(C_5H_5)$, (b) cluster $Ti_2:(C_8H_8)Ti(C_5H_5)Ti(C_8H_8)$, (c) cluster $Ti_3:(C_8H_8)Ti(C_5H_5)Ti(C_8H_8)Ti(C_5H_5)$, and (d) cluster $Ti_4:(C_8H_8)Ti(C_5H_5)Ti(C_8H_8)Ti(C_5H_5)Ti(C_8H_8)$ sandwiched between gold electrodes. The black and red lines stand for minority and majority spin channels, respectively. Inset: The corresponding structures. (e) Schematic plot of the spin-transport device of Ti_3 where a cluster Ti_3 is connected with the left- and right-electrode Au(100) leads.

highly effective spin filters. We examine four geometry clusters of $Ti_1:(C_8H_8)Ti(C_5H_5)$, $Ti_2:(C_8H_8)Ti(C_5H_5)Ti(C_8H_8)$, $Ti_3:(C_8H_8)Ti(C_5H_5)Ti(C_8H_8)Ti(C_5H_5)$, and $Ti_4:(C_8H_8)Ti(C_5H_5)Ti(C_8H_8)Ti(C_5H_5)Ti(C_8H_8)$. As shown in the inset in Figs. 2(a)–2(d), the device structure consists of two semi-infinite gold electrodes sandwiching each cluster Ti_n ($n = 1$–4). The detailed structure of the spin-transport device of Ti_3 is shown in Fig. 2(e), and cluster Ti_3 is connected with gold (100) leads on the left- and right-hand sides. The gold electrodes extend to $z = \pm\infty$ along the transport direction and extend with the large vacuum layer in the transverse x and y directions in order to suppress the interaction between the device and its mirror images. For example, we first determine the energetically favorable connect geometry of the cluster Ti_3 on a Au(100) surface through vacuum. Therefore, in the investigated molecular junctions, the optimized Ti_3 are connected to the sites of left and right electrodes via transport direction 14.57 Å, which is the maximum binding energy. The self-consistently calculated source-drain I-V characteristics are shown in Figs. 2(a)–2(d). The spin currents are found to vary nonlinearly as a function of the bias V_b. This feature is caused by transport resonance, which is mediated by a combination of molecular states and the gold electronic structure. As shown in Figs. 2(a) and 2(c), the spin-up and spin-down currents in Ti_1 and Ti_3 structures are similar, with negligible differences. This indicates small spin polarization in both structures. However, in Ti_2 and Ti_4 structures, the spin-up current is significantly larger than the spin-down current, with the latter completely suppressed by the bias voltage, as shown in Figs. 2(b) and 2(d). Calculations show that the spin-filtering effect of four tunnel junctions is 0.01%, 82.3%, 59.1%, and 100%, respectively, where clusters Ti_2 and Ti_4 exhibit a much greater spin-polarized transport.

In order to further explain the transport phenomena, we use the molecular orbital to analyze the relaxed atomic structure described in the NEGF DFT study above. We can clearly see the difference in the four clusters, as shown in Fig. 3, from the molecular projected self-consistent Hamiltonian (MPSH) of the two main transmission channels, the highest occupied molecular orbital (HOMO) and the lowest unoccupied molecular orbital (LUMO). For the Ti_1 cluster, all spatial distribution for HOMO orbitals of the spin-up and spin-down channel comes from d_{z^2} and is localized around the titanium atom. This is consistent with the results of x-ray diffraction [27], and we can see that the LUMOs are almost the same for the two channels, although not so localized. It results in a near-zero spin polarization.

Regarding the cluster of Ti_3, although the orbital distribution is delocalized, the frontier orbital distributions for the different spin channels are very similar to

Spin channel / Molecular	Up		Down		Magnetic moment (μB)
	HOMO	LUMO	HOMO	LUMO	
(Ti_1) C_8TiC_5	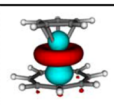	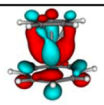	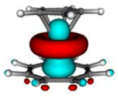	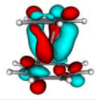	1
(Ti_2) $C_8TiC_5TiC_8$	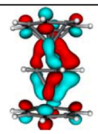	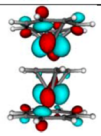	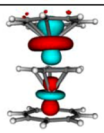	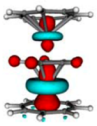	0.03
(Ti_3) $C_8TiC_5TiC_8TiC_5$	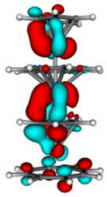	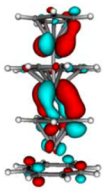	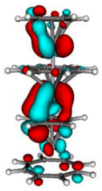	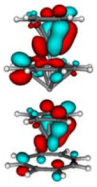	1.19
(Ti_4) $C_8TiC_5TiC_8TiC_5TiC_8$	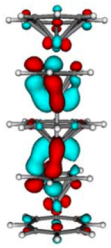	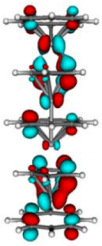	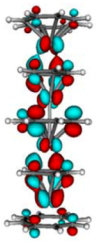	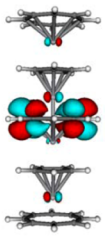	2.27

FIG. 3. MPSH of HOMO and LUMO molecular orbitals and the magnetic moment for four finite length sandwich clusters, respectively.

the Ti_1. For the Ti_2 cluster, all spatial distributions for the HOMO and LUMO orbitals of the spin-down channel come from the d_{z^2} orbital and are localized around the titanium atom. However, for the spin-up channel, all orbital states are delocalized and distributed on both carbon atoms and bonds. Therefore, it greatly enhances the conductivity. The spatial distribution for the Ti_4 cluster is similar to Ti_2. Only the spin-up channel of the molecular magnetization can flow through the Ti_4 molecular junction, which exhibits a very high spin polarization with an efficiency approaching 100%. In addition, the magnetic moments of the four molecules display an "n" number in odd-even oscillation behavior ($n = 1$–4). According to Peierls' transition theorem, the chain of 1D equally spaced would undergo a distortion. The structural analysis of these molecules (in Fig. 4) shows that the neighboring Cp-Ti and COT-Ti reorganize as pairing units and display an oscillatory unit distance. This distortion is symmetrical to the center of the molecular chain, which is quite different for odd and even numbers of Ti atoms. This difference leads to the magnetic moment oscillation.

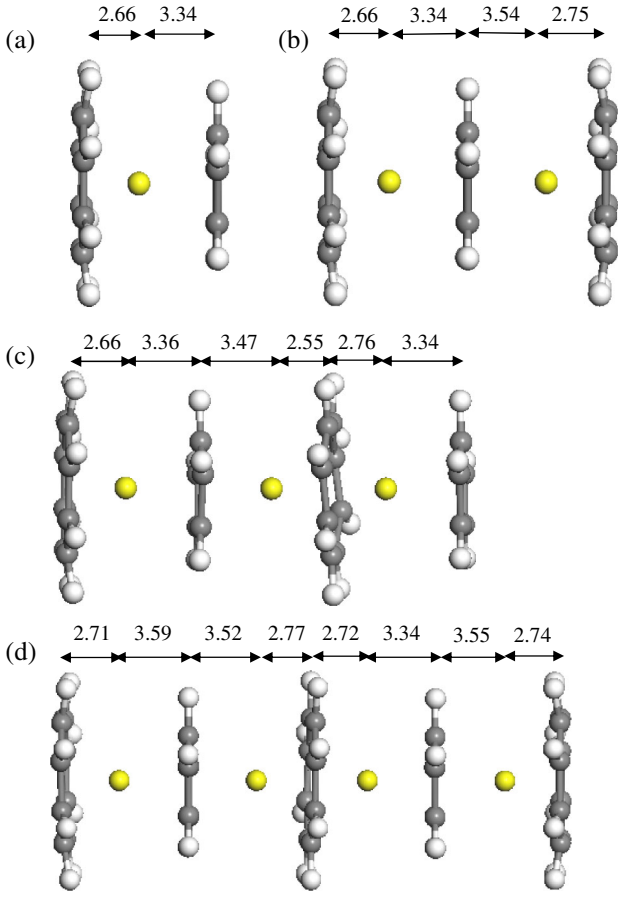

FIG. 4. Structures of the finite-sized finite $[C_5H_5TiC_8H_8]_n$ multidecker molecules at the ground state. The distances (Å) between Ti atoms and aromatic rings are marked. (a) Cluster $Ti_1 : (C_8H_8)Ti(C_5H_5)$, (b) cluster $Ti_2 : (C_8H_8)Ti(C_5H_5)Ti(C_8H_8)$, (c) cluster $Ti_3 : (C_8H_8)Ti(C_5H_5)Ti(C_8H_8)Ti(C_5H_5)$, and (d) cluster $Ti_4 : (C_8H_8)Ti(C_5H_5)Ti(C_8H_8)Ti(C_5H_5)Ti(C_8H_8)$. Yellow sphere, Ti atom; gray sphere, C atom; white sphere, H atom.

Since the odd and even numbers of titanium atom clusters possess different polarizations, we calculate the I-V characteristics of the spin antiparallel configuration (APC) with a low-spin state for Ti_2, Ti_3, and Ti_4 junctions. We also calculate the spin parallel configuration (PC) with a high-spin state, as shown in Fig. 5(a). Interestingly, the total currents for PC and APC are very different for the Ti_4 junction, while those for the Ti_2 and Ti_3 junction show similar variation trends. In the Ti_4 junction, the PC current starts to increase rapidly at a low bias and approaches saturation as the applied bias increases. The PC current starts to rise again when the bias increases beyond 0.75 V. On the other hand, the current of the APC spin setup is close to zero at the entire bias range of [−0.75 V, 0.75 V]. As a result, the Ti_4 junction possesses a large tunneling magnetoresistance (TMR) ratio. This is defined as $\mathrm{TMR} = [(I_{\mathrm{PC}} - I_{\mathrm{APC}})/I_{\mathrm{APC}}] \times 100\%$, as shown in Fig. 5(b), where I_{APC} and I_{PC} are the total currents for PC and APC at the same bias, respectively. TMR of around $(10^5)\%$ is obtained at a close to zero bias by using equilibrium conductance. This behavior shows that the device at the Ti_4 junction can also be used as an organic spin valve.

To gain further insight into the transport mechanism in these structures, we calculate the spin-dependent transmission spectra as a function of electron energy E and bias voltage for the Ti_4 junction. The transmission spectra of the charge and spin transport with the PC and APC setup of spin alignment are shown in Figs. 5(c) and 5(d). In a PC state, the transport peak enters the bias window in the low-bias range of [−0.2 V, 0.2 V], leading to a rapid increase of current shown in Fig. 5(a). However, when the bias is higher than 0.4 V, the transmission remains unchanged in the bias window, resulting in current saturation. When bias increases further to more than 0.75 V, the bias window again catches the transmission of positive energy, leading to another rapid increase of current. In the APC setup, no transmission enters the bias window of [−0.75 V, 0.75 V], leading to suppression of the APC current. When the bias increases further, only a small portion of the transmission spectra moves into the bias window, and then the APC current increases by only a small amount. As a result, up to $(10^5)\%$ TMR based on the single-molecule magnet tunnel junctions of $Ti_4 : (C_8H_8)Ti(C_5H_5)Ti(C_8H_8)Ti(C_5H_5)Ti(C_8H_8)$ can be obtained. In addition, all the calculations performed here are within the scope of coherent transport at 300 K temperature. For our low-dimensional systems, where charging and electron-phonon couplings are neglected, it arises due to various electronic features including orbital alignment.

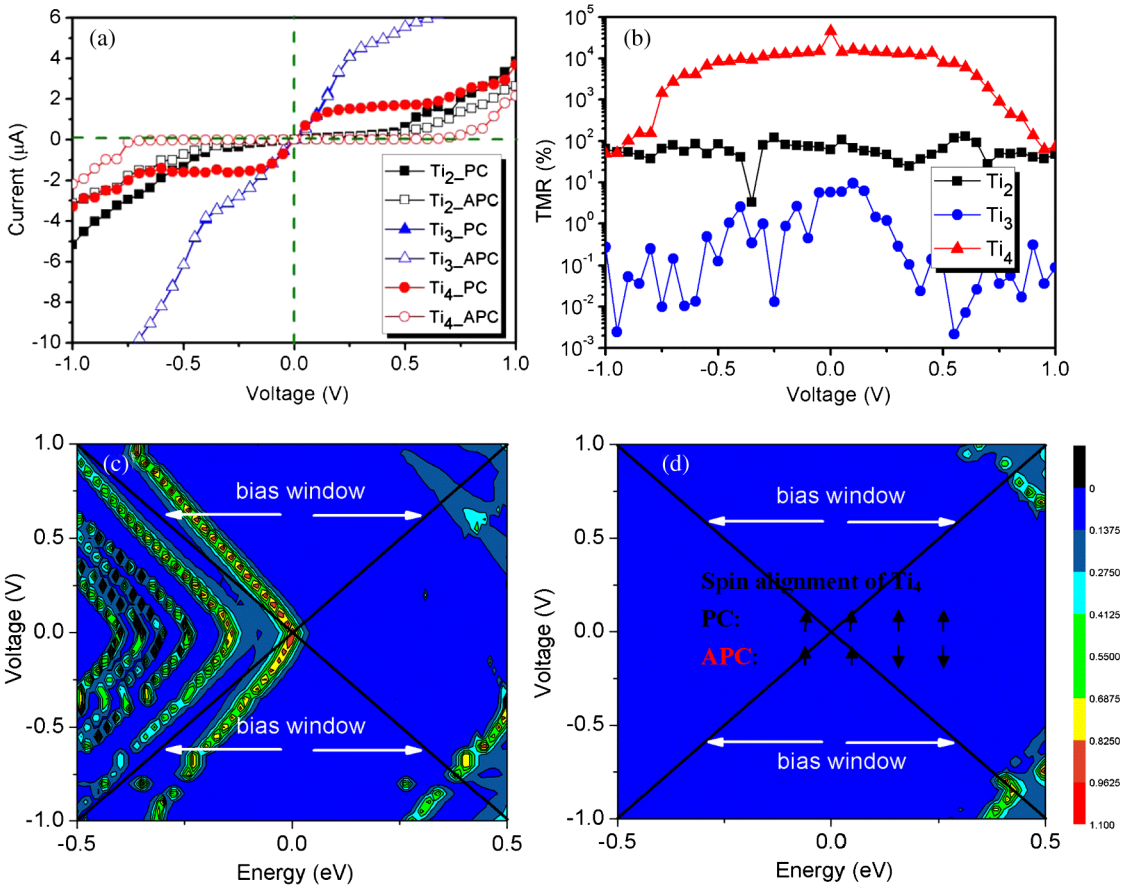

FIG. 5. (a) *I-V* curves for the PC and APC setup of the spin alignment for $Ti_2:(C_8H_8)Ti(C_5H_5)Ti(C_8H_8)$, $Ti_3:(C_8H_8)Ti(C_5H_5)Ti(C_8H_8)Ti(C_5H_5)$, and $Ti_4:(C_8H_8)Ti(C_5H_5)Ti(C_8H_8)Ti(C_5H_5)Ti(C_8H_8)$ clusters sandwiched between two Au(100) surfaces. Black (solid symbols), Ti_2 PC setup ↑↑; black (hollow symbols), APC setup ↑↓; blue (solid symbols), Ti_3 PC setup ↑↑↑; blue (hollow symbols), APC setup ↑↑↓; red (solid symbols), Ti_4 PC setup ↑↑↑↑; red (hollow symbols), APC setup ↑↑↓↓. (b) TMR of the same device as a function of bias. TMR $= [(I_{PC}\text{-}I_{APC})/I_{APC}]100\%$. (c),(d) Spin-dependent transmission spectrum as a function of electron energy E and bias voltage for the Ti_4 junction, respectively, for the PC (c) and APC (d) setup of the spin alignment. The up and down triangles shown by the intersecting solid straight lines are the bias windows which set boundaries for transmission that contributes to the current at a given bias voltage. The Fermi energy is set to zero.

IV. CONCLUSIONS

In conclusion, this study systematically investigates the structural, electronic, and spin properties of one-dimensional $(\eta^5\text{-}C_5H_5)Ti(\eta^8\text{-}C_8H_8)$ wires by using density-functional theory. The one-dimensional $(\eta^5\text{-}C_5H_5)Ti(\eta^8\text{-}C_8H_8)$ wires studied have the same pattern, with the two nearest-neighboring carbon rings parallel to each other. The Ti atoms aligning in the center point of the ring show half-metallic features at the ground spin state.

We perform a first-principles study on the electronic transport properties of a one-dimensional organic cluster $(\eta^5\text{-}C_5H_5)Ti(\eta^8\text{-}C_8H_8)Ti$ molecular junction. Theoretical results indicate that these devices can also be used as a large spin valve and spin filter with efficiency approaching 100%. Furthermore, an ultrahigh TMR ratio of around 10^5 is obtained in the Ti_4 junction. This study demonstrates that these SWMs and clusters have interesting electronic and magnetic properties with great potential for future nanoelectronics and spintronic applications.

ACKNOWLEDGMENTS

The authors acknowledge the support from the China Postdoctoral Science Foundation Funded Project (Project No. 2014M562009) and National Natural Science Foundation of China under Grants No. 11404121 and No. 11404119.

[1] S. Sen and S. Chakrabarti, Ferromagnetically coupled cobalt-benzene-cobalt: The smallest molecular spin filter with unprecedented spin injection coefficient, J. Am. Chem. Soc. **132**, 15334 (2010).

[2] W. J. Cho, Y. Cho, S. K. Min, W. Y. Kim, and K. S. Kim, Chromium porphyrin arrays as spintronic devices, J. Am. Chem. Soc. **133**, 9364 (2011).

[3] J. Zhou, J. L. Sonnenberg, and H. B. Schlegel, Theoretical studies of $An_2^{II}(C_8H_8)_2$ (An = Th, Pa, U, and Np) complexes: The search for double-stuffed actinide metallocenes, Inorg. Chem. **49**, 6545 (2010).

[4] Z. Xie, T. Z. Markus, S. R. Cohen, Z. Vager, R. Gutierrez, and R. Naaman, Spin specific electron conduction through DNA oligomers, Nano Lett. **11**, 4652 (2011).

[5] D. A. Stewart, A new type of magnetic tunnel junction based on spin filtering through a reduced symmetry oxide: FeCo|$Mg_3B_2O_6$|FeCo, Nano Lett. **10**, 263 (2010).

[6] G. Zhang, R. Zhou, Y. Gao, and X. C. Zeng, Silicon-containing multidecker organometallic complexes and nanowires: A density functional theory study, J. Phys. Chem. Lett. **3**, 151 (2012).

[7] H. Wang, Z. Sun, Y. Xie, R. B. King, and H. F. Schaefer, Analogues of the Lavallo–Grubbs compound Fe(CH): Equilateral, isosceles, and scalene metal triangles in trinuclear cyclooctatetraene complexes M(CH)of the first row transition metals (M = Ti, V, Cr, Mn, Fe, Co, and Ni), Inorg. Chem. **50**, 9256 (2011).

[8] C. J. O. Verzijl and J. M. Thijssen, DFT-based molecular transport implementation in ADF/BAND, J. Phys. Chem. C **116**, 24393 (2012).

[9] A. S. Ivanov, K. V. Bozhenko, and A. I. Boldyrev, On the suppression mechanism of the Pseudo-Jahn–Teller effect in middle E_6 ($E = P$, As, Sb) rings of triple-decker sandwich complexes, Inorg. Chem. **51**, 8868 (2012).

[10] W. J. Cho, Y. Cho, S. K. Min, W. Y. Kim, and K. S. Kim, J. Am. Chem. Soc. **133**, 9364 (2011).

[11] L. Z. Li, R. Qin, H. Li, L. L. Yu, Q. H. Liu, G. F. Luo, Z. X. Gao,, and J. Lu, Functionalized graphene for high-performance two-dimensional spintronics devices, ACS Nano **5**, 2601 (2011).

[12] D. Aravena and E. Ruiz, Coherent transport through spin-crossover single molecules, J. Am. Chem. Soc. **134**, 777 (2012).

[13] K. Miyajima, A. Nakajima, S. Yabushita, M. B. Knickelbein, and K. Kaya, Ferromagnetism in one-dimensional vanadium-benzene sandwich clusters, J. Am. Chem. Soc. **126**, 13202 (2004).

[14] J. Wang, P. H. Acioli, and J. Jellinek, Structure and magnetism of V_nBz_{n+1} sandwich clusters, J. Am. Chem. Soc. **127**, 2812 (2005).

[15] H. Xiang, J. Yang, J. G. Hou, and Q. Zhu, One-dimensional transition metal-benzene sandwich polymers: Possible ideal conductors for spin transport, J. Am. Chem. Soc. **128**, 2310 (2006).

[16] V. V. Maslyuk, A. Bagrets, V. Meded, A. Arnold, F. Evers, M. Brandbyge, T. Bredow, and I. Mertig, Organometallic Benzene-Vanadium Wire: A One-Dimensional Half-Metallic Ferromagnet, Phys. Rev. Lett. **97**, 097201 (2006).

[17] M. Koleini, M. Paulsson, and M. Brandbyge, Efficient Organometallic Spin Filter between Single-Wall Carbon Nanotube or Graphene Electrodes, Phys. Rev. Lett. **98**, 197202 (2007).

[18] L. P. Zhou, S. W. Yang, M. F. Ng, M. B. Sullivan, V. B. C. Tian, and L. Shen, One-dimensional iron-cyclopentadienyl sandwich molecular wire with half metallic, negative differential resistance and high-spin filter efficiency properties, J. Am. Chem. Soc. **130**, 4023 (2008).

[19] J. F. Yang, L. P. Zhou, Q. Han, and X. F. Wang, Bias-controlled giant magnetoresistance through cyclopentadienyl–iron multidecker molecules, J. Phys. Chem. C **116**, 19996 (2012).

[20] L. Wang, Z. X. Cai, J. Y. Wang, J. Lu, G. F. Luo, L. Lai, J. Zhou, R. Qin, Z. X. Gao, S. P. Yu, G. P. Li, W. N. Mei, and S. Sanvito, Novel one-dimensional organometallic half metals:vanadium-cyclopentadienyl, vanadium-cyclopentadienyl-benzene, and vanadium-anthracene wires, Nano Lett. **8**, 3640 (2008).

[21] S. C. Zhu, H. H. Fu, G. Y. Gao, S. L. Wang, Y. Ni, and K. L. Yao, Perfect spin filtering and large spin thermoelectric effects in organic transition-metal molecular junctions, J. Chem. Phys. **139**, 024309 (2013).

[22] F. A. Cotton and G. Wilkinson, *Advanced Inorganic Chemistry* (Wiley, New York 1988), Vol. 5.

[23] W. Moffitt, Electronic structure of biscyclopentadienyl compounds, J. Am. Chem. Soc. **76**, 3386 (1954).

[24] J. D. Dunitz and L. E. Orgel, Electronic Structure of metal bis-cyclopentadienyls, J. Chem. Phys. **23**, 954 (1955).

[25] M. Elian, M. M. L. Chen, D. M. P. Mingos, and R. Hoffmann, Comparative bonding study of conical fragments, Inorg. Chem. **15**, 1148 (1976).

[26] D. W. Clack and K. D. Warren, Metal-ligand bonding in 3d sandwich complexes, Struct. Bond. **39**, 1 (1980).

[27] J. Weber, A. Goursot, E. Pénigault, J. H. Ammeter, and J. Bachmann, Electronic structure of metallocene compounds. 3. Comparison of the results of multiple-scattering $X\alpha$ calculations with various electronic observables of cobaltocene, J. Am. Chem. Soc. **104**, 1491 (1982).

[28] Z. F. Xu, Y. Xie, W. L. Feng, and H. F. Schaefer, Systematic investigation of electronic and molecular structures for the first transition metal series metallocenes $M(C_5H_5)_2$ (M = V, Cr, Mn, Fe, Co, and Ni), J. Phys. Chem. A **107**, 2716 (2003).

[29] Y. Yamaguchi, W. Ding, C. T. Sanderson, M. L. Borden, M. J. Morgan, and C. Kutal, Electronic structure, spectroscopy, and photochemistry of group 8 metallocenes, Coord. Chem. Rev. **251**, 515 (2007).

[30] A. Boccia, A. G. Marrani, S. Stranges, R. Zanoni, M. Alagia, M. Cossi, and M. F. Iozzi, Symmetry breaking effect in the ferrocene electronic structure by hydrocarbon-monosubstitution: An experimental and theoretical study, J. Chem. Phys. **128**, 154315 (2008).

[31] A. Nakamurac and N. Hagihara, Cyclopentadienyl cobalt cyclooctatetraene, Bull. Chem. Soc. Jpn. **33**, 425 (1960).

[32] H. O. Van Oven and H. J. de Liefde Meijer, Cyclopentadienylcyclooctatetraenetitanium, J. Organomet. Chem. **19**, 373 (1969).

[33] H. Wang, X. H. Chen, Y. Xie, R. B. King, and H. F. Schaefer, Mixed sandwich compounds $C_5H_5MC_8H_8$ of the first-row transition metals: Variable hapticity of the eight-membered ring, Organometallics **29**, 1934 (2010).

[34] H. Braunschweig, M. Fuss, T. Kupfer, and K. Radacki, Selective dilithiation of $[Ti(\eta^5\text{-}C_5H_5)(\eta^8\text{-}C_8H_8)]$ and subsequent conversion into neutral and cationic ansa-complexes, J. Am. Chem. Soc. **133**, 5780 (2011).

[35] M. D. Segall, P. J. D. Lindan, M. J. Probert, C. J. Pickard, P. J. Hasnip, S. J. Clark, and M. C. Payne, First-principles simulation: Ideas, illustrations and the CASTEP code, J. Phys. Condens. Matter **14**, 2717 (2002).

[36] J. M. Soler, E. Artacho, J. D. Gale, and A. Garca, The SIESTA method for ab initio order-N materials simulation, J. Phys. Condens. Matter **14**, 2745 (2002).

[37] J. Taylor, H. Guo, and J. Wang, Ab initio modeling of quantum transport properties of molecular electronic devices, Phys. Rev. B **63**, 245407 (2001).

[38] M. Brandbyge, J. L. Mozos, J. Taylor, and K. Stokbro, Density-functional method for nonequilibrium electron transport, Phys. Rev. B **65**, 165401 (2002).

[39] S. K. Nielsen, M. Brandbyge, K. Hansen, K. Stokbro, J. M. Van Ruitenbeek, and F. Besenbacher, Current-Voltage Curves of Atomic-Sized Transition Metal Contacts: An Explanation of Why Au is Ohmic and Pt is Not, Phys. Rev. Lett. **89**, 066804 (2002).

[40] J. Huang, Q. X. Li, H. Ren, H. B. Su, and J. L. Yang, Single quintuple bond [PhCrCrPh] molecule as a possible molecular switch, J. Chem. Phys. **125**, 184713 (2006).